

Optical manipulation of complex molecular systems by high density green photons: experimental and theoretical evidence

Sorin Comorosan^{1,2}, Silviu Polosan^{3,a}, Irinel Popescu⁴, Ioan Stamatini⁵, Elena Ionescu², Sorin Avramescu⁶, Liviu Cristian Cune¹, and Marian Apostol¹

¹ Department of Theoretical Physics, National Institute for Physics and Nuclear Engineering, 077125 Magurele, Romania

² Interdisciplinary Research Group, Romanian Academy, 010071 Bucharest, Romania

³ Materials & Multifunctional Structures, National Institute of Materials Physics, 077125 Magurele, Romania

⁴ Academy of Medical Sciences, 077125 Bucharest, Romania

⁵ Department of Biophysics, University of Bucharest, 077125 Bucharest, Romania

⁶ Department of Chemistry, University of Bucharest, 077125 Bucharest, Romania

Received 22 January 2013 / Received in final form 6 February 2013

Published online 29 May 2013 – © EDP Sciences, Società Italiana di Fisica, Springer-Verlag 2013

Abstract. The recent revolution in modern optical techniques revealed that light interaction with matter generates a force, known as *optical force*, which produces material properties known in physics as *optical matter*. The basic technique of the domain uses forces exerted by a strongly focused beam of light to trap small objects and subsequently to manipulate their local structures. The purpose of this paper is to develop an alternative approach, using irradiations with high-density-green-photons, which induce electric dipoles by polarization effects. The materials used for the experiments were long carbon chains which represent the framework of biological macromolecules. The physical techniques used to reveal the locally induced molecular arrangements were: dynamic viscosity, zeta potential, chemiluminescence, liquid chromatography; mass spectrometry, and Raman and infrared spectroscopy. The principal result of our experiments was the detection of different molecular arrangements within the mixture of alkane chains, generated by our optical manipulations. This induced “optical matter” displayed two material properties: antioxidant effects and large molecular aggregation effects. In order to bring the experimental results in relation with theory, we developed a physical model and the interacting force between polarizable bodies was computed. By numerical calculations stable structures for $N = 6$ and $N = 8$ particles were obtained.

1 Introduction

A relevant scientific interest developed recently in a high-lighted domain of physics, known as *mesoscopia*. Mesoscopic systems encompass force scales from femto-to-nano newtons, length scales from nano-to-micro meters and time scales from microseconds and upwards. It is an interesting field with many nonlinear phenomena, particularly within the realm of basic processes, such as cellular respiration, reproduction and signaling. Within this context, a revolution in optical manipulation was reported [1], concerning our means for organizing and analyzing mesoscopically textured matter, with the requested level of rigorous access and control. The basic technique, known as *optical tweezers* was created at Bell Laboratories by Ashkin et al. [2]. Optical tweezers use the forces of a focused beam of light to trap small objects and subsequently to rearrange their mesoscopic framework. The scientific relevance of manipulation with optical tweezers for basic research is far reaching. A series of technical feats

was reported: direct measurements of macromolecular interactions in solution [3], fluctuation analysis of single enzyme-kinetics [4], the study of magnetic flux lines in superconductors [5], oscillatory colloidal interactions [6] and even results which relate to the very core of physics, such as transient violations of the second law of thermodynamics by hydrodynamic fluctuations [7]. This is the scientific context in which we advance a novel approach for the optical manipulation of complex macromolecular systems. Our technology uses high-density-green-photon beams (HDGP) instead of tweezers formed from focused laser beams. High density photon fluxes induce multiphoton processes that generate metastable systems, which may be conveniently studied ex situ, after photoexcitation.

The irradiation of complex structures with HDGP induces electric dipoles by polarization effects. The induced dipoles interact with an external electromagnetic field and with one another, leading to *new organized material structures*, such as molecular aggregates and micro-particles. We term this type of matter, obtained by HDGP-optical manipulation, *complex optical matter*.

^a e-mail: silv@infim.ro

The optical manipulation with collimated HDGP-beams is particularly suited for complex structures (macromolecules and cells). It covers a larger area than focused tweezers and is capable of organizing mesoscopic matter into a new 3D molecular architecture.

In a detailed study by circular dichroism on a complex protein (bovine serum albumin), we revealed a new 3D structure of the ellipticity (i.e. the α -helix content of the polypeptide chain), induced in the molecule by HDGP-irradiations, exhibiting new biological properties [8]. A series of similar preliminary experimental results, obtained with HDGP irradiations of chemical and cellular systems, was also reported [9]. In previous studies, we have reported that within the electromagnetic visible domain, green photons ($\lambda = 510\text{--}540$ nm) display in their reactions a highest quantum yield, as compared with the blue and red domain [10]. The prevalence of green light effects within the visible domain was also recently reported in cellular systems [11]. The purpose of this paper is to undertake an in-depth study of possible new 3D structures induced by HDGP in well-defined molecules and revealed through rigorous physical methods. We used long carbon chains (alkanes) which represent the framework of biological macromolecules. The alkane mixtures are adequate for this type of experiments, since they do not conduct electricity and produce a series of carbon-radicals under thermal degradation that may be rigorously measured. The physical techniques used to reveal the locally induced new mesoscopically textured matter were: dynamic viscosity, zeta potential, chemiluminescence, liquid chromatography, and a series of spectroscopic methods; i.e. mass spectrometry and Raman and infrared spectroscopy. In order to relate our experimental results to theory, we put forward a physical model which is based on the polarization charge, the current densities and the interacting force between polarizable bodies.

2 Experimental methods

2.1 Irradiation procedure

The GL (green light) irradiation was performed with bright (1000 lumens) light-emitted diodes (LEDs) of, mounted on ventilated copper radiators. In this setup, monochromatic light of $\lambda = 514$ nm was obtained, with intensities up to 4×10^5 Lx, as measured by a digital Luxmeter LX-1102, Lutron. For each experiment, the GL-irradiation was tuned to deliver a standard flux of 10^4 Lx.

2.2 Thermal degradation of mineral oil

A defined volume of mineral oil for each type of experiment was placed on two dishes (control & probe) and kept for 30 min in an electrical oven at 165°C . To increase the oxidation rate, a foil of aluminium, used as catalytic agent, was added to the samples. The probe was exposed to green light through a small hole in the roof of

the oven. After 30 min the dishes were taken out for the measurements. The geometry and the progression of the experiments were rigorously arranged to be similar for the control and the probe in all the experimental set-ups.

2.3 Viscosity measurements

Viscosity was determined using a Malvern Vibro Viscometer SV-10 with an accuracy of 1% over the full range of $0.3\text{--}10^4$ mPas. The calibration technique uses purified water as a standard. The SV-10 has a built-in function to measure the purified water temperature and compute its viscosity vs. temperature.

2.4 Zeta potential

The determination of the zeta potential was realized with a Malvern NanoZetasizer ZEN3600 particle analyzer, using a He-Ne laser with transmission attenuation scaled from 100% to 0.0003%. The conductivity domain ranged from 0 to 200 mS/cm, and the particle size domain ranged between 5 nm–10 μm . A volume of 0.5 ml of mineral oil was introduced into the 3 ml instrument cell for recording.

2.5 Chemiluminescence

Measurements were performed with a chemiluminescence basic instrument from ACL-instruments-CH-3210 Kerzers-Switzerland. The data were acquired and recorded to within an accuracy of ± 0.02 . From the chemiluminescence recordings the induction and maximum times for a complete oxidation, the initial and maximum chemiluminescence intensity and the oxidation rate were computed. For this particular experimental set-up a series of GL fluxes with intensities up to 10^5 Lx was used.

2.6 Liquid chromatography

A Varian LC-instrument was used, with the 1322 GC capillary technique and a CP-Sil5CB column. Temperature $40\text{--}310^\circ\text{C}$, $10^\circ\text{C}/\text{min}$, carrier gas He, 40 KPa (0.4 bar, 5.7 psi). Temperature programmed on-column injector FID, $T = 340^\circ\text{C}$ detector. Sample size 5 μl . Solvent sample petroleum ether 40–60.

2.7 Mass spectrometry

A Shimadzu LCMS 2010EV mass spectrometer with electrospray ionization, one step-quadrupole mass analyser, data acquisition in the range of m/z 200 to 1000 and a scan speed of 1000 amu/s was used. The mobile phase was acetonitrile (99.98% purity), with a gas flow of 0.4 ml/min. The LCMS was operated in positive acquisition mode with the nebulizing gas flow set at 1.5 l/min. The CDL (curve

desolvation line) temperature was 250 °C, with an applied voltage of -5 V. The heat block temperature was set at 200 °C, the interface voltage was set at 3.5 kV and the detector voltage was set at 1.5 kV. The sample was obtained by mixing 10 μ l mineral of oil with 1 ml of acetonitrile (99,98% purity), and then ultrasonicated for 20 min in an ultrasonic bath. A volume of 20 μ l of sample was injected into the LCMS.

2.8 Raman spectroscopy

Raman spectra were recorded using a Jasco NRS 3100 with a 532 nm laser, a 1 cm^{-1} resolution, a spectral range from 50 to 8000 cm^{-1} , 10 spectra accumulation, a central wavenumber 1049.71 cm^{-1} and a holographic grating with 1200 grooves/mm. The measurements were performed in a reflective mode using Petri dishes ($\phi = 30$ mm). A quantity of 1 ml of mineral oil was used in the control and the probe samples.

2.9 FTIR spectroscopy

IR- spectra were obtained on a Bruker Vertex 70 FT-IR spectrophotometer, using a single reflection ATR device.

2.10 Quantum computations

Gaussian 03 W provides the most advanced modelling capabilities of electronic structures, starting from the fundamental laws of quantum mechanics by using B3LYP functional, 6–311 g basis sets and geometric connectivity, the electronic properties of alkanes were modelled. A full population analysis was achieved. The charge density computations of butane and ketone molecules were performed with Chemisian.

3 Main findings

3.1 Viscosity

Viscosity is a method which may prove the formation of large aggregates generated by HDGP-irradiation. The mineral oil is a mixture of components with different mass fractions and different densities. In our experiments, the probe under HDGP manipulations displayed an increased viscosity as a result of an aggregation process. At 302 K, the sample viscosity was 45.2×10^{-3} N s m^{-2} , clearly higher the control value of 42.8×10^{-3} N s m^{-2} .

It is known that GL is only weakly absorbed by alkane molecules under normal conditions, which indicates a certain absence of electronic-transition processes. The absorption may increase under thermal degradation. Therefore, it is likely that GL electrically polarizes the alkane macromolecules by changing the molecular charge distribution. Theoretical intermolecular potential functions for alkanes are described in reference [12]. Hence,

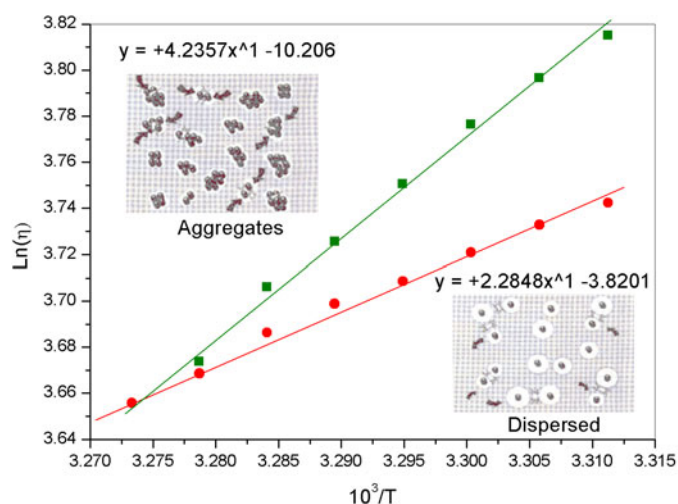


Fig. 1. Temperature dependence of dynamic viscosity measurements. Determinations on thermally degraded mineral oil (165 °C) with the Vibro Viscometer SV-10, using purified water as a standard. In this experimental set-up, a 50 ml volume sample is used.

a dipole interaction may develop between the respective molecules. These dipoles interact with the external electromagnetic field and, through their own polarization field, amongst each-other, leading to dipole chains/string structures. This does explain the increase in the viscosity of the HDGP-irradiated samples and the generation, by this optical manipulation, of a new mesoscopic texture within the molecular mixture (see an optical representation in the inset of Fig. 1). In our viscosity experimental set-up, a linear dependence of the dynamic viscosity was observed for 302–305.5 K temperature range (see Fig. 1).

Similar linear behaviour has been observed for methane, ethane and propane within the range of 223–373 K [13].

The temperature dependence of the viscosity obeys the Arrhenius equation, whose logarithm obeys:

$$\ln \eta = \ln \eta_0 + \left(\frac{E_a}{R} \right) \frac{1}{T}, \quad (1)$$

where η_0 is the viscosity at 302 K and E_a can be interpreted as a viscous flow activation energy. The slope of the linear dependence indicates the resistance to shear deformation. For the probe $E_a = 35.2$ J K^{-1} mol^{-1} and for the control sample $E_a = 18.9$ J K^{-1} mol^{-1} . The high viscosity in the case of our irradiated samples indicates a smaller deformation, which thus may favour large aggregates as a result of the HDGP optical manipulation.

The experiments reported here may open new perspective on research in the field. In particular, the optical manipulation technique may reveal new types of transport parameters in a series of dense fluids that may be appropriately investigated [14]. Within the same context let us mention the reported effects on viscosity of orientational order in branched and normal alkanes [15]. This technique may be used to generate new mesoscopic textures in different oils as well as monitoring the orientational order of the

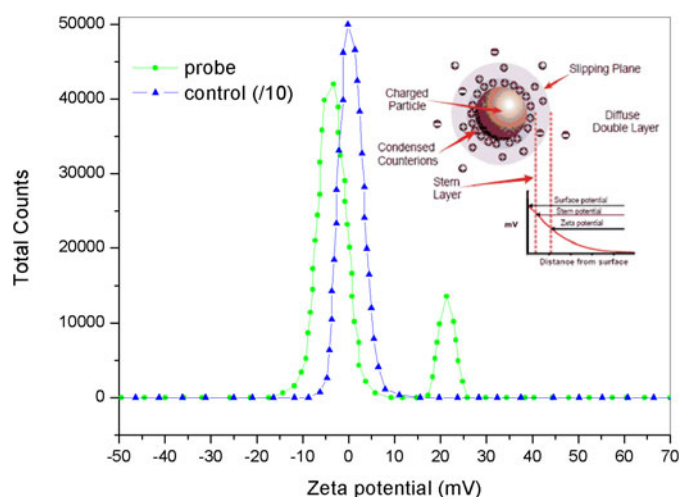


Fig. 2. Zeta potential recordings. The recording of thermally degraded mineral oil (165 °C) under HDGP exhibits two peaks at -3.5 mV and 21.4 mV. The control sample presents a single peak at -0.15 mV one order of magnitude higher than the sample peak. The inset presents the standard double layer model.

oil components. This opens the possibility to determine and control viscosity which may prove valuable to the oil industry.

3.2 Zeta potential

Zeta potential is a technique for measuring the magnitude of the electrostatic charge and the repulsion/attraction between particles. The values of the zeta potential represent fundamental parameters of structural stability. It constitutes a significant method for studying aggregation and mobility. In zeta potential determination the molecules irradiated with HDGP are surrounded by oppositely polarized particles, forming a fixed layer. Outside it a series of opposite polarity molecules generates an electrical double layer (Fig. 2-inlet).

Our experimental results reveal that the zeta potential curve of the thermally degraded mineral oil, under HDGP, displays a second peak at $+21.4$ mV, as compared with the control experiment (see Fig. 2). This peak indicates an incipient aggregation process, induced in the probe sample by optical manipulation. This process is also revealed by our viscosity results. As expected the electrical conductivity during the zeta potential measurements decreases from 2.45×10^{-4} S/cm in the control sample to a smaller value of 1.84×10^{-4} S/cm. This behaviour suggests the formation of large aggregates.

In the thermally degraded control the large peak centred at -0.15 mV can be connected with the significant quantity of carbonyl groups produced under the degradation process. Under similar thermal conditions, the HDGP optical manipulation of the probe reduces the carbonyl concentration by an order of magnitude. This is a direct proof of oxidative process inhibition. The shift of the carbonyl zeta potential peak to -3.5 mV may indicate

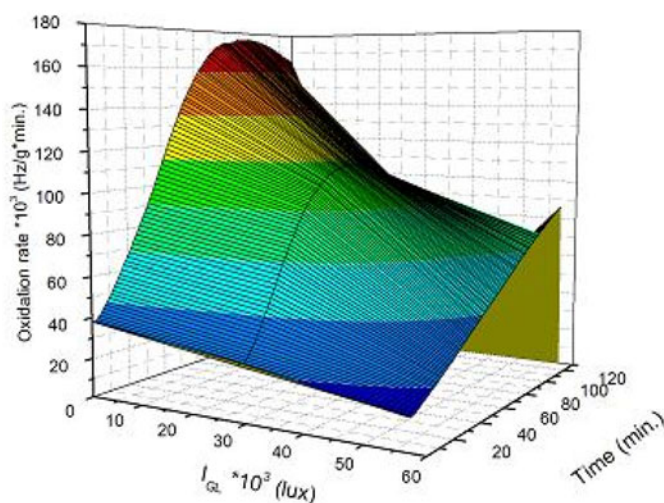


Fig. 3. 3D-representation of chemiluminescence measurements for HDGP-irradiated thermally degraded (165 °C) mineral oil. The Oz -axis represents the oxidation rate. The Oy -axis represents the green photon intensities. The Ox -axis represents the irradiation time dependence of the oxidation rate. Both intensities and time dependencies have an exponential behavior. The oxidation rate is expressed as Hz g^{-1} .

a modification of the electrical double layer, which influences the molecular aggregate's mobility.

3.3 Chemiluminescence

Chemiluminescence represents the generation of electromagnetic radiation in the form of light by the release of energy from its underlying chemical reaction. In our experimental set-up, 2 ml of thermally degraded mineral oil were introduced in the CL basic instrument CH-3210 and the kinetic parameters were recorded. The alkane oxidation rate, as determined experimentally, is given by:

$$V_{ox} = ke^{-aI}. \quad (2)$$

The chemiluminescence variation shows an oxidation rate decrease as a function of increasing HDGP intensity (I). A large relaxation constant " a " indicates a strong decrease in the oxidation rate on the first HDGP-irradiation steps. The time dependence of the oxidation rate under HDGP indicates a slow oxidation process, reducing the reaction time (Fig. 3).

At zero HDGP flux density, the oxidation rate is constant. The drastically reduced oxidation rate with increasing HDGP flux, suggests the presence of a non-linear effect of exponential decay type. All these results indicate an HDGP inhibitory effect on the mineral oil thermal degradation. We reproduce here the results obtained with zeta potential determinations, when an oxidative process inhibition appears as a property of the new mesoscopic texture, generated by optical manipulation.

The chemiluminescence technique is a common method for determining reactive oxygen species. In the alkane case, the transition between chain branching peroxy-chemistry, the concerted elimination and β -scission reactions control the overall reactivity of the

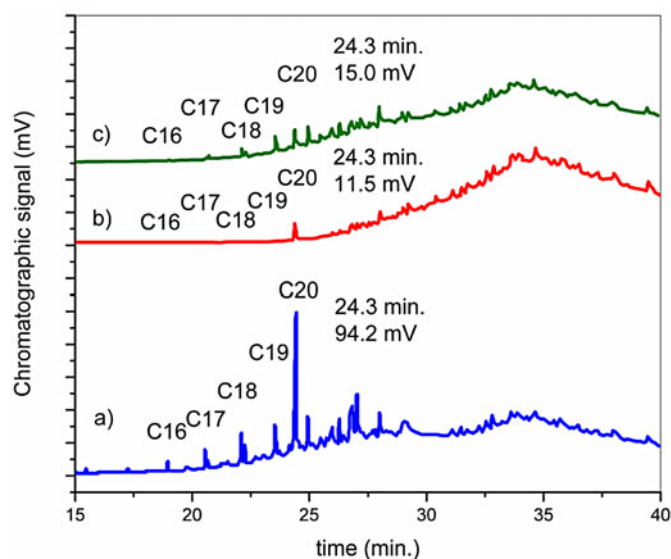


Fig. 4. Chromatographic area of low fraction hydrocarbons distribution. On the *Ox*-axes represents the heating time of the mineral oil, separated on the non-polar CP SIL 5 CB and converted to temperature from the heating slope of $7^\circ\text{C}/\text{min}$. The flame ionization detector (FID) records the ionized fractions as a potential in mV.

oxidation system. A comprehensive chemical kinetics of alkane oxidation has recently been reported [16]. Our scheme may prove useful for this type of kinetics under optical controlled manipulation.

3.4 Liquid chromatography

Mineral oil consists mainly of hydrocarbons which may be separated on a CP-Sil 5CB column using the method described in reference [17]. The identification of carbon chains from C_{10} – C_{40} is realized on standard Chromopack maps (Chromopack Application Rep. 96–50).

Figure 4 shows the results obtained by liquid chromatography of the mineral oil, C_{20} = peak, in the control sample (Fig. 4a), in the probe under thermal degradation (Fig. 4b) and in the probe with the addition of HDGP (Fig. 4c). The values of the liquid chromatographic probes are recorded as potentials. They were 94.2 mV for the control, 11.5 mV for the thermally degraded probe and 15.0 mV for the HDGP probe. This is a significant result. It demonstrates the expected changes of physical parameters (elution peaks) in the thermally degraded probe versus the HDGP ones, and, moreover, reveals a different makeup in the chemical composition of the probe under optical manipulation.

3.5 Mass spectroscopy

When an alkane is ionized by an electromagnetic field it loses an electron and forms a radical cation with the same mass as the parent compound. It represents the molecular ion (M^+). The alkane molecular ion may fragment further, to form a homologous series of cations with $\text{C}_n\text{H}_{2n+1}$

mass, mainly by the loss of methyl and ethyl radicals. This is the mechanism on which mass determinations in alkane mixtures are based. The mass spectrometric fragmentation of *n*-alkanes is by now well understood [18]. The mass spectra of macromolecules allow the analysis of high molecular weight, using mass-to-charge ratio (m/z). These spectra correspond to a statistical distribution of consecutive peaks, characteristic of multiple charged molecular ions, obtained through protonation or deprotonation. An ion separated from the central one by $(j - 1)$ peaks, in increasing order of mass-to-charge ratio, has a mass m_2 and a charge number $(z_1 - j)$ so that:

$$(z_1 - j)m_2 = M + (z_1 - j)m_p, \quad (3)$$

where M denotes the molecular mass and m_p is the proton mass.

These parameters may be used to uncover possible charges in the distribution of different species within the mineral oil mixture.

In our experiments, the control of the mass-to-charge distribution displays two fitted Gaussian peaks as compared with a single Gaussian one for the HDGP-irradiated probe.

The thermally degraded mineral oil exhibits two statistical distributions, with characteristic peaks, the first centered at $m/z = 531$ and the second one at $m/z = 619$ (cf. Fig. 5a). The difference between the central peak located at 619 and the value obtained for the $j = 3$, being situated at 707, is a multiple of the carbonyl mass (88).

The thermally degraded mineral oil, under HDGP manipulation, (Fig. 5b) exhibits a quite distinct behaviour.

The mass spectrometry pattern reveals a single statistical distribution, centered at $m/z = 525$, being close to the control value. The difference between the peak at 525, and the one corresponding to $j = 2$, located at 569, is the carbonyl mass value (44). The HDGP irradiation induces a single species of alkane, which undergoes the oxidative process. The optical manipulation of the probe displays again a modification of its mesoscale architecture. Let us emphasize that the HDGP induced texture acquires new properties. In this case, a clear antioxidant effect one a single species of alkanes as being revealed by the oxidative process.

3.6 Vibrational spectroscopy

Vibrational spectroscopy is the technique used to determine vibrational, rotational, and low frequency modes in a system. In this study, we used Raman and FTIR spectroscopies. In the Raman spectrum, the thermal degradation of mineral oil does not affect the 1450 cm^{-1} and 2840 – 2990 cm^{-1} C-H vibrations.

The concentrations of hydroxyl groups (3200 , 3400 cm^{-1}) and of the carbonyl one peak (1760 cm^{-1}) are increased. The HDGP-irradiation reduces the carbonyl and hydroxyl concentrations during the thermal degradation process (see Fig. 6a).

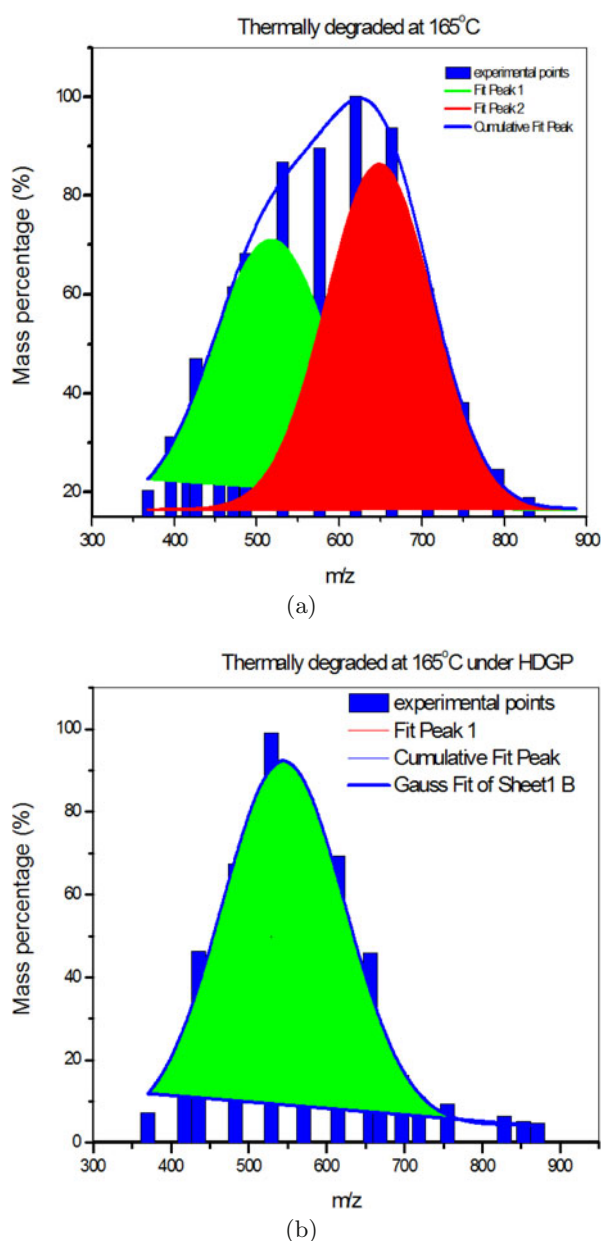


Fig. 5. Mass spectra of multiply charged ions. (a) Mass-to-charge-ratio (blue bars) of thermally degraded mineral oil (165 °C). (b) Mass-to-charge-ratio (blue bars) of thermal degraded mineral oil (165 °C) under HDGP. The two fitted Gaussian curves in the thermally annealed sample peak at 531 and 619 m/z . Under HDGP the thermally annealed sample exhibits only one fitted curve centered at 531 m/z .

The hydroxyl and carbonyl intensities of the probe reveal reduced values with respect to the control experiment, suggesting a clear antioxidant effect. A similar behaviour may be observed in the FTIR spectrum (Fig. 6b) for which the carbonyl stretching frequency is 1719 cm^{-1} . The absorption bands of the hydroxyl group and the carbonyl group are reduced in the samples when exposed to HDGP during the oxidation in air, suggesting again an antioxidant effect.

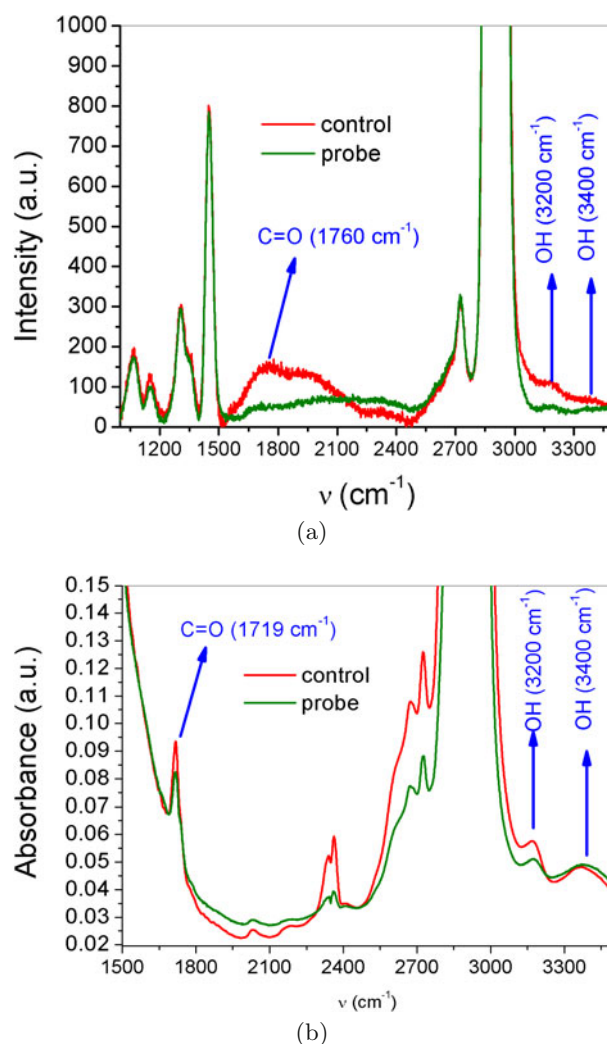
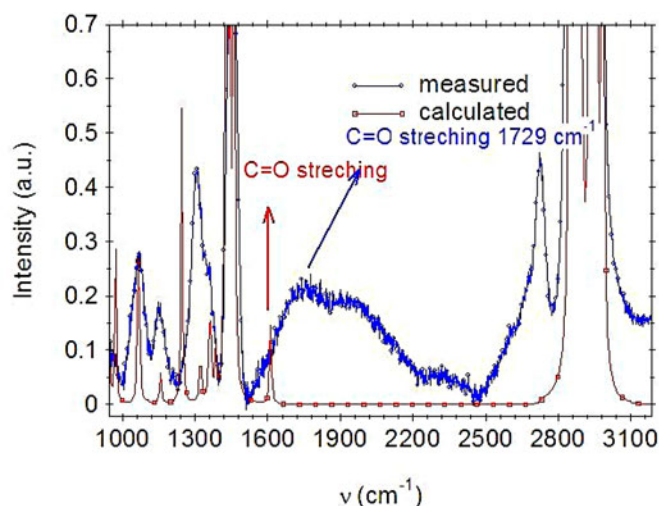


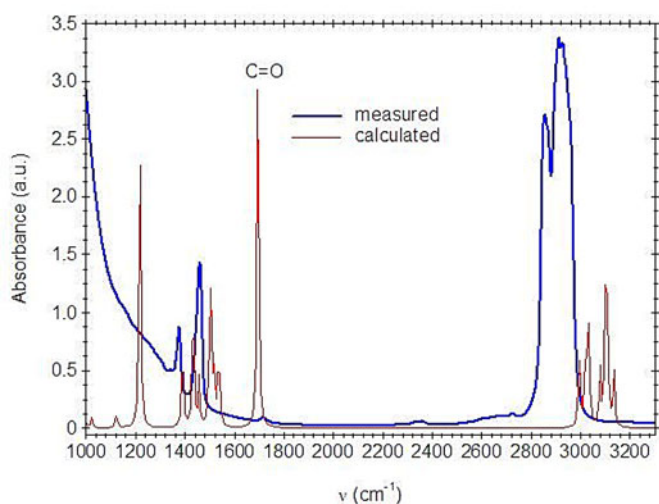
Fig. 6. (a) Raman spectra of the control sample and of the probe sample manipulated by HDGP; (b) FTIR spectra of the control sample and of the probe sample manipulated by HDGP.

3.7 Quantum chemical modeling

A detailed quantum computation was performed in order to investigate the theoretical basis for the alkane oxidation process. The calculations were performed using Gaussian 03 W with Chemisian software on the butane molecule and on its oxidized ketone form. The optimizations of the two structures were performed using density functional theory (DFT) which computes the electron correlations by using general functionals. These corresponding functionals screen the electronic energy into several Hamiltonians, taking into account the kinetic energy, the electron-nuclear interaction, the Coulomb repulsion, and an exchange-correlation term accounting for the remaining part of the electron-electron interaction. The DFT method also allows the prediction of IR and Raman spectra for the butane structure. The computed Raman spectrum is presented in Figure 7a. A good agreement with experimental data is observed.



(a)



(b)

Fig. 7. (a) Calculated Raman curves using DFT modeling for butane structure, together with the experimental spectra; (b) calculated FTIR curves using DFT modeling for butane structure, together with the experimental spectra.

The simulated FTIR spectrum yields reasonable positions for carbonyl stretching as compared to the Raman one, which is slightly shifted to a lower frequency (cf. Fig. 7b).

The oxygen in the ketone molecule has a large area of electronegativity around it, which will induce a polarization, i.e. a higher reactivity. In the butane molecule, the absence of oxygen lowers the reactivity, preserved by the HDGP-irradiation, which generates molecular aggregates that will in turn deter the oxidative processes. The oxidized ketone forms due to its electronegativity, induces a high reactivity. The absence of oxygen resulting in alkanes under HDGP turns the molecules into less reactive species.

The density of states for these two structures and the HOMO and LUMO orbitals for the butane molecule are represented in Figure 8.

We have suggested a tentative physical mechanism for these interesting experimental results. Light interaction with a system is determined by the dielectric polarization density, expressed as a Taylor series as follows:

$$P_i/\varepsilon_0 = \sum_j \chi_{ij}^{(1)} E_j + \sum_{j,k} \chi_{ijk}^{(2)} E_j E_k + \sum_{j,k,l} \chi_{ijkl}^{(3)} E_j E_k E_l + \dots, \quad (4)$$

with ε_0 the vacuum dielectric constant. The third term describes multi-photon processes, proportional to E^3 and 10^{-3} efficiency from the power of incident light. This explains the need for intensive light to obtain such processes, which was exactly the set-up of our experimental models, using powerful LED's.

The HDGP irradiation may induce the formation of polarized macromolecules, in a quantum macroscopic cooperative effect, which generates the large aggregates revealed by our experiments. These may represent a direct experimental proof for the existence of stable quantum macroscopic structures, unentangled with the environment.

3.8 Theoretical considerations

3.8.1 Polarization force

Let us consider an external monochromatic electric field

$$\mathbf{E}(\mathbf{r}, t) = \frac{1}{2} [\mathbf{E}(\mathbf{r})e^{i\Omega t} + \mathbf{E}^*(\mathbf{r})e^{-i\Omega t}] \quad (5)$$

and the associated magnetic field

$$\mathbf{H}(\mathbf{r}, t) = \frac{ic}{2\Omega} [\text{curl}\mathbf{E}(\mathbf{r})e^{i\Omega t} - \text{curl}\mathbf{E}(\mathbf{r})e^{-i\Omega t}] \quad (6)$$

(derived from $\text{curl}\mathbf{E} = -(1/c)\partial\mathbf{H}/\partial t$). The polarization induced by such an electric field in a point-like body placed at \mathbf{R} is given by:

$$\mathbf{P}(\mathbf{R}, t) = \frac{1}{2} [\alpha^*(\Omega)\mathbf{E}(\mathbf{R})e^{i\Omega t} + \alpha(\Omega)\mathbf{E}^*(\mathbf{R})e^{-i\Omega t}]. \quad (7)$$

This polarization induces charge and current densities

$$\begin{aligned} \rho(\mathbf{r}, t) &= -v [\mathbf{P}(\mathbf{R}, t)\text{grad}] \delta(\mathbf{r} - \mathbf{R}), \\ \mathbf{j}(\mathbf{r}, t) &= v \frac{\partial \mathbf{P}(\mathbf{R}, t)}{\partial t} \delta(\mathbf{r} - \mathbf{R}) \end{aligned} \quad (8)$$

for a point-like particle of volume v placed at \mathbf{R} . The Lorentz force acting due to the field upon these charges and currents is:

$$\mathbf{F} = \int d\mathbf{r} \rho(\mathbf{r}, t)\mathbf{E}(\mathbf{r}, t) + \frac{1}{c} \int d\mathbf{r} \mathbf{j}(\mathbf{r}, t) \times \mathbf{H}(\mathbf{r}, t). \quad (9)$$

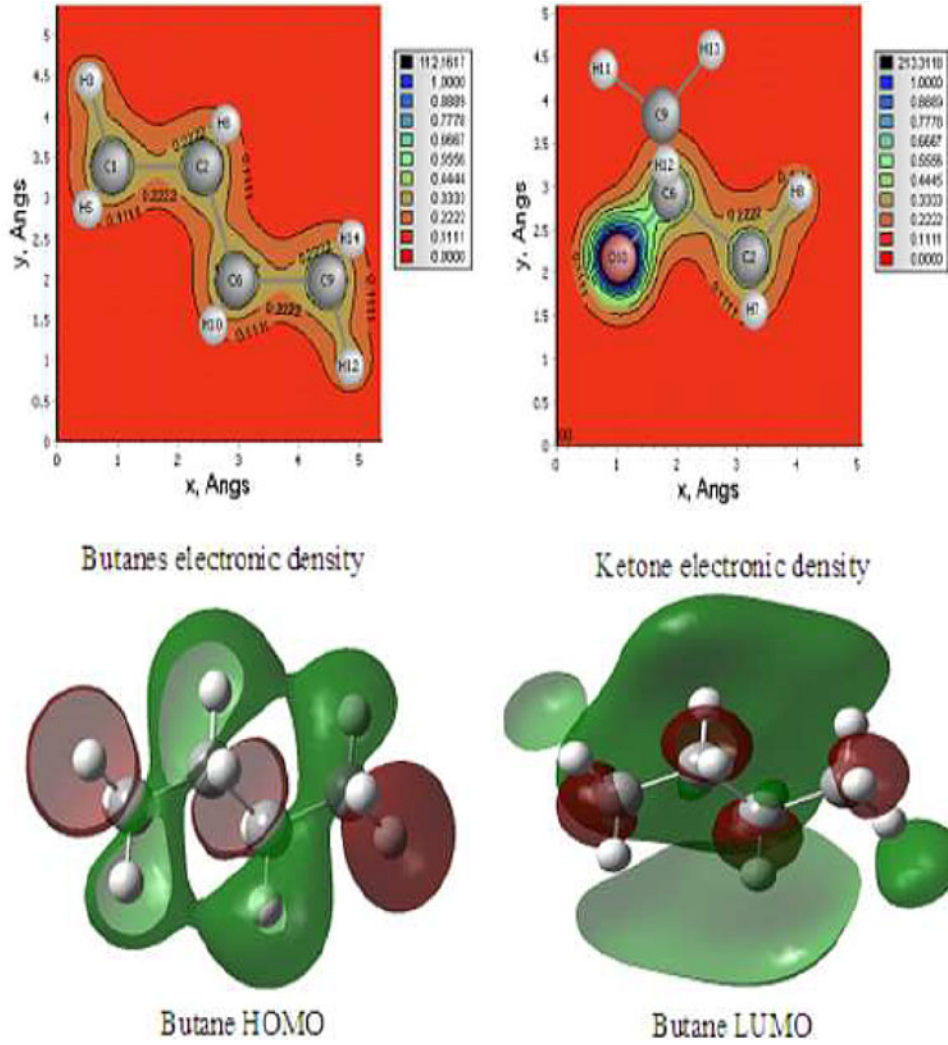


Fig. 8. Charge density computation of butane and ketone molecules. The oxidized ketone form, due to its electronegativity, induces a high reactivity. The lack of oxygen, resulting in alkanes under HDGP, turns the molecules into less reactive species. The respective HOMO and LUMO orbitals are shown.

By using the external fields given by equations (5) and (6) and the charge and current densities given by equations (8), we get

$$\mathbf{F}(\mathbf{R}) = \frac{v}{4}\alpha^*(\Omega) \{ [\mathbf{E}(\mathbf{R})\text{grad}]\mathbf{E}^*(\mathbf{R}) + \mathbf{E}(\mathbf{R}) \times \text{curl}\mathbf{E}^*(\mathbf{R}) \} + c.c. \quad (10)$$

For real polarizabilities, we get for the time average of this force

$$\mathbf{F}_{ext}(\mathbf{R}) = \frac{v}{4}\alpha(\Omega)\text{grad}|\mathbf{E}(\mathbf{R})|^2 \quad (11)$$

(the imaginary part of the polarizability is related to the damping coefficient).

This is the well-known force experienced by a (point-like) dielectric (polarizable matter) due to an external field. For a plane wave $\mathbf{E}(\mathbf{r}) = e^{-i\mathbf{k}\mathbf{r}}$, where $k = \Omega/c$, we can see that the external force vanishes.

3.8.2 Optical force

Let us consider two point-like polarizable bodies, one located at \mathbf{R} (body 1) and another located at the origin (body 2). All the quantities pertaining to these two bodies are denoted by labels 1 and 2, respectively.

An external field polarizes the bodies, and induces charges and currents. These polarization charges and currents produce in turn their own electromagnetic fields which act upon them. Following the lines described above, we get the force,

$$\mathbf{F} = \frac{v_1 v_2}{2\pi T} \int d\omega \alpha_1^*(\omega) \alpha_2(\omega) E_i^*(\omega; \mathbf{R}) E_j(\omega; \mathbf{R} = 0) \times \left(\frac{\omega^2}{c^2} \delta_{ij} + \frac{\partial^2}{\partial R_i \partial R_j} \right) \frac{\partial}{\partial \mathbf{R}} \frac{e^{i\frac{\omega}{c}R}}{R}, \quad (12)$$

where summations are performed over the components i and j . We can see that the force given by these equations is a generalization of the static dipolar force (it contains

frequency-dependent factors); we may call it a dynamic dipolar force. In the static limit $\omega \rightarrow 0$ using (static) polarizations $\mathbf{P}_{1,2}$, we can check that this force is proportional to $\mathbf{F} = -\partial U/\partial \mathbf{R}$, where

$$U = \frac{\mathbf{P}_1 \mathbf{P}_2}{R^3} - \frac{3(\mathbf{P}_1 \mathbf{R})(\mathbf{P}_2 \mathbf{R})}{R^5} \quad (13)$$

is the static dipolar interaction energy.

It is also worth noting that equation (12) leads to the well-known *optical force* in the wave-zone $\omega R/c \gg 1$. In this case, we may retain only the spatial derivatives of the exponential in equation (12). Assuming for simplicity a monochromatic external field \mathbf{E}^{ext} parallel with \mathbf{R} , acting upon both bodies, we immediately obtain the interaction energy of the two bodies from equation (12), $U \sim v_a v_b (\omega/c)^2 |E|^2 (\cos \omega R/c)/R$, which is the typical result corresponding to the optical force [1,2].

We estimate the interaction force given by equation (12) by using an external field of the form given in equation (5). The calculations are straightforward (we use $\delta(\omega = 0) = T/2\pi$), and we get

$$\begin{aligned} \mathbf{F} = & \frac{1}{4} v_1 v_2 \alpha_1(\Omega) \alpha_2^*(\Omega) \left\{ \frac{\Omega^2}{c^2} \mathbf{E}^*(\mathbf{R}) \mathbf{E}(\mathbf{R} = 0) \right. \\ & \left. + [\mathbf{E}^*(\mathbf{R}) \text{grad}] [\mathbf{E}(\mathbf{R} = 0) \text{grad}] \right\} \\ & \times \frac{\partial}{\partial \mathbf{R}} \frac{e^{-i\frac{\Omega}{c}R}}{R} + c.c. \end{aligned} \quad (14)$$

We get a simplification by assuming $\mathbf{E}(\mathbf{R}) = \mathbf{E} e^{-i\mathbf{k}\mathbf{R}}$, as for a plane wave ($\mathbf{k}\mathbf{E} = 0$, $k = \Omega/c$); in addition, we assume identical particles ($v_1 = v_2 = v$) and real polarizabilities $\alpha_1 = \alpha_2 = \alpha = \alpha^*$:

$$\mathbf{F} = \frac{1}{4} v^2 \alpha^2 e^{i\mathbf{k}\mathbf{R}} \left\{ \lambda^2 E^2 + (\mathbf{E} \text{grad})^2 \right\} \frac{\partial}{\partial \mathbf{R}} \frac{e^{-i\lambda R}}{R} + c.c., \quad (15)$$

where $\lambda = \Omega/c$.

Introducing $\mathbf{x} = \lambda \mathbf{R}$, equation (15) can be written more conveniently as:

$$\begin{aligned} \mathbf{F} = & \frac{1}{2} v^2 \alpha^2 \lambda^4 E^2 \frac{\mathbf{x}}{x} \left[- \left(\frac{1}{x} - \frac{3}{x^3} \right) \sin(x - \mathbf{n}\mathbf{x}) \right. \\ & \left. - \left(\frac{2}{x^2} - \frac{3}{x^4} \right) \cos(x - \mathbf{n}\mathbf{x}) \right] \\ & + \mathbf{E} \frac{\mathbf{E}\mathbf{x}}{x} \left[-2 \left(\frac{1}{x^2} - \frac{3}{x^4} \right) \cos(x - \mathbf{n}\mathbf{x}) \right. \\ & \left. + \frac{6}{x^3} \sin(x - \mathbf{n}\mathbf{x}) \right] \\ & + \frac{(\mathbf{E}\mathbf{x})^2 \mathbf{x}}{x^3} \left[\left(\frac{1}{x} - \frac{15}{x^3} \right) \sin(x - \mathbf{n}\mathbf{x}) \right. \\ & \left. + 3 \left(\frac{2}{x^2} - \frac{5}{x^4} \right) \cos(x - \mathbf{n}\mathbf{x}) \right], \end{aligned} \quad (16)$$

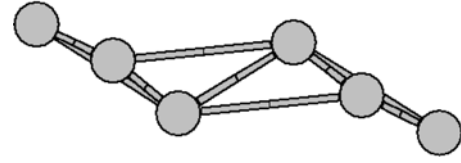


Fig. 9. A stable structure for $N = 6$ particles. The shortest inter-particle distance corresponds to $R \approx 0.5\lambda$.

where $\mathbf{n} = \mathbf{k}/k = c\mathbf{k}/\Omega$. In the wave zone, $x \gg 1$, the force given above becomes

$$\mathbf{F} \simeq -\frac{1}{2} v^2 \alpha^2 \lambda^4 \left[E^2 - \frac{(\mathbf{E}\mathbf{x})^2}{x^2} \right] \frac{\mathbf{x}}{x^2} \sin(x - \mathbf{n}\mathbf{x}). \quad (17)$$

This is a long-range, rapidly oscillating force (it decreases as $\sim 1/x$), which is vanishing both along \mathbf{E} and \mathbf{k} ($\mathbf{E}\mathbf{k} = 0$). This is a significant result. It reveals one of a few $1/R$ type forces induced by the electromagnetic field in complex macromolecular structures.

3.8.3 Localized new structures, induced by optical manipulation, in mesoscopia

The interaction force between two particles given by equation (16) can be written as:

$$\mathbf{F} = \mathbf{F}^{drift} + \mathbf{F}^{coh}, \quad (18)$$

where

$$\mathbf{F}^{drift} = \frac{1}{2} v^2 \alpha^2 \lambda^4 \left[E^2 - \frac{(\mathbf{E}\mathbf{x})^2}{x^2} \right] \frac{\mathbf{x}}{x^2} \cos(x) \sin(\mathbf{n}\mathbf{x}), \quad (19)$$

and

$$\mathbf{F}^{coh} = -\frac{1}{2} v^2 \alpha^2 \lambda^4 \left[E^2 - \frac{(\mathbf{E}\mathbf{x})^2}{x^2} \right] \frac{\mathbf{x}}{x^2} \sin(x) \cos(\mathbf{n}\mathbf{x}). \quad (20)$$

The forces given by equation (19) act as a drifting force, the total force acting on a two particle system being $2F^{drift}$. For larger structures it can also act as a stress force, deforming the stable structures obtained with the cohesion forces given by equation (20). The force \mathbf{F}^{coh} has zeros which, when reached by moving the particles along the forces, give rise to stable structures. These structures can move away under the influence of the total drifting force. For two particles, the repulsive regions alternate with attractive regions, giving the obvious stable distances $x = k\pi$ and many others due to the presence of the $\cos(\mathbf{n}\mathbf{x})$ term. Neglecting the drifting forces and using the interaction given by equation (20), we have investigated numerically the existence of stable structures for multi-particle systems.

In Figures 9 and 10, we present two stable structures obtained with the cohesion forces given by equation (20).

Accordingly, an external electromagnetic field (plane wave) can induce dipoles in matter which interact with

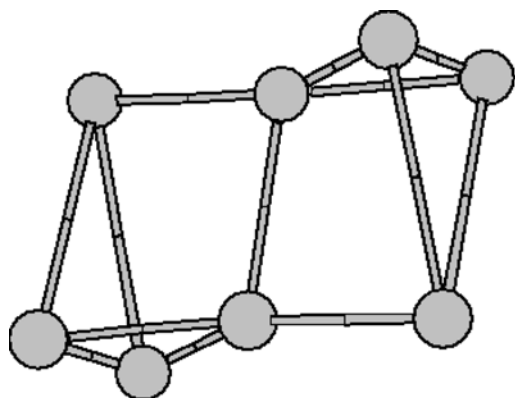


Fig. 10. A stable structure for $N = 8$ particles. The shortest inter-particle distance corresponds to $R \approx 0.6\lambda$.

a force capable of binding them in chains oriented along the direction of the electric field. This organization of polarizable matter, subjected to the action of the electromagnetic field, is called optical matter in physics. In the bound state, the macromolecular chains (filaments) have a different electronic structure, which makes them more robust to external aggressions. In addition, the induced optical matter may exhibit an increased viscosity, and different physical characteristics, as observed experimentally. All these properties are subject to further investigation.

4 Main conclusions

In this paper, we have presented an alternative to the optical manipulation of matter with optical tweezers. Our technique uses irradiation with collimated HDGP-beams, better suited for complex macromolecular systems. They cover larger areas and are capable of organizing them into heterogeneous hierarchically structured 3D mesoscopic textures. We have shown that these newly generated 3D structures acquire new physical properties. We underline the revealed anti-oxidant properties, significant for biology and medicine; introduce for the first time the electromagnetic field as a possible alternative to chemical anti-oxidant treatments. Based on our experimental results, we extended here the significance of the term *optical matter*, previously described at the nano-scale level, to complex structures. In our previously published results, we revealed the same modification of mesoscopic

texture under optical manipulation of biological macromolecules [8,9]. Hence, we may extend the significance of the “optical matter” notation to *biological optical matter*.

Our work underlines the visible domain of electromagnetic field’s (particularly green light) significance and the respective induced polarization effects in technologies dominated by electronic transition processes.

This work was supported by National Research Plan of Romania, Grant Bios-ADN 81-082, Grants TDRCPP 22, PN-II-139/05.10.2011 and PN-II-ID-PCE-2011-3-0769.

References

1. D.G. Grier, Nature **424**, 810 (2003)
2. A. Ashkin, J.M. Dziedzic, J.E. Bjorkholm, S. Chu, Opt. Lett. **11**, 288 (1986)
3. J.C. Crocher, D.G. Grier, Phys. Rev. Lett. **73**, 352 (1994)
4. K. Svoboda, P.P. Mitra, S.M. Block, Proc. Natl. Acad. Sci. **91**, 11782 (1994)
5. P.T. Korda, G.C. Spalding, D.G. Grier, Phys. Rev. B **66**, 024504 (2002)
6. R. Verma, J.C. Crocker, T.C. Lubenski, A.G. Yodh, Macromolecules **33**, 177 (2000)
7. G.M Wang, E.M. Sevick, E. Mittag, D.J. Searles, D.J. Evans, Phys. Rev. Lett. **89**, 050601 (2002)
8. S. Comorosan, S. Polosan, I. Popescu, E. Ionescu, R. Mitrica, L. Cristache, A.E. State, Eur. Biophys. J. **39**, 1483 (2010)
9. S. Comorosan, S. Polosan, S. Jipa, I. Popescu, G. Marton, E. Ionescu, L. Cristache, D. Badila, R. Mitrica, J. Photochem. Photobiol. B **102**, 39 (2011)
10. S. Comorosan, in *Progress in Theoretical Biology*, edited by R. Rosen (Academic Press, New York, 1976), p. 161
11. E.M. Vink, B.J. Cagnie, M.J. Cornelissen, H.A. Declercq, D.C. Cambier, Lasers Med. Sci. **18**, 95 (2003)
12. X. Wangshen, P. Jingzi, D. Alexander, J. McKerell, G. Jiali, J. Chem. Theor. Comput. **3**, 1878 (2007)
13. C.J. Seeton, Tribology Lett. **22**, 67 (2006)
14. M.J. Assael, J.H. Dymond, M. Papadaki, P.M. Patterson, Int. J. Thermophys. **13**, 269 (1992)
15. G. Delmas, P. Purves, P. Saint Domain, J. Phys. Chem. **79**, 1970 (1975)
16. S.M. Sarathy, Combustion & Flame **158**, 2338 (2011)
17. M. Vasudevan, J. Ravi, S. Ravisankar, B. Suresh, J. Pharm. Biomed. Anal. **25**, 77 (2001)
18. A. Lavanchy, R. Houriet, T. Gaumann, J. Mass. Spectr. **14**, 79 (1979)